Pergamon

Int. J. Heat Mass Transfer. Vol. 37, No. 6, pp. 927–938, 1994

0017–9310/94 $6.00 + 0.00

0017–9310(93)E0016–A

Density inversion effect on transient natural convection in a rectangular enclosure

WEI TONG† and JEAN N. KOSTER‡

Department of Aerospace Engineering Sciences, University of Colorado, Boulder, CO 80309, U.S.A.

(*Received* 3 *March* 1993 *and in final form* 15 *October* 1993)

Abstract—Transient natural convection in a water layer subjected to density inversion is studied numerically by a finite element method. The results illustrate that the temperature difference which determines the position of the maximum density plane in the water layer, can alter flow field and heat transfer substantially. The significant effect of aspect ratio on transient natural convection is also investigated. The heat transfer is maximized in a square enclosure and is less at other aspect ratios.

1. INTRODUCTION

IN STUDIES of transient flow in an enclosure, interest is commonly directed toward the following issues: (i) the evolution of convective flow pattern and temperature field with time; (ii) the time scale leading to steady-state conditions; (iii) oscillatory or monotonic approach to steady-state conditions; (iv) the thickness of the boundary layer at the vertical wall when the flow approaches steady state, and (v) the characteristic velocity within this boundary layer.

Most transient studies were done with Boussinesq fluids, i.e. fluids exhibiting linear density as a function of temperature. Landis and Yanowitz [1] conducted experiments on transient natural convection in a narrow vertical cell of aspect ratio $A \gg 1$. As the Rayleigh number increases, temperature profiles across the cavity first show a conduction-type regime and eventually develop boundary layer type flow. Patterson and Imberger [2] analyzed the transient process in a cavity of $A \leqslant 1$ with differentially heated end walls. By utilizing scaling analysis they found that the flow reaches steady state at a time scale $\tau \sim L^2/\kappa A Ra^{1/4}$, where the Rayleigh number is defined with height. Their numerical results substantiated the existence of an oscillatory transition to the final steady-state conditions. Bejan *et al.* [3] reported experimental data of high-Rayleigh-number convection in a horizontal cavity with a small aspect ratio ($A = 0.0625$). Their results showed that at high Rayleigh number the core flow structure is non-parallel and characterized by intrusion layers (jets) lining the two horizontal walls. This transition is governed by the parameter $Ra^{1/4}A$, with $Ra^{1/4}A < 1$ as a necessary condition for parallel core flow.

A theoretical transient analysis of high Rayleigh number convection in a square cavity was performed by Han [4]. The heat transfer rate was found to be oscillatory during a transient period leading to steady state. Further experimental studies were conducted by Ivey [5]. Nicolette *et al.* [6] and Hall *et al.* [7] performed a numerical and experimental investigation for transient cooling in an isothermal square enclosure with one vertical wall cooled, and the other three walls insulated. Good agreement was found between experimental data and numerical predictions.

It is known that for some fluids (e.g. water, liquid helium, HgCdTe) density is not a monotonic function of temperature, instead, density reaches its maximum at a specific temperature and decreases when deviating from this temperature. As a result, the Boussinesq approximation, which is based on the linear behavior of the density–temperature relation, is not applicable to these fluids. This character, known as density inversion, can significantly change the flow field and heat transport in an enclosure. Natural convection in such a liquid is of practical importance in areas such as atmospheric and oceanic movement, ice forming and melting, crystal growth, etc. Though the density inversion effect on natural convection has been studied extensively in the past [8–12], the vast majority of these studies considered steady-state flows in enclosures.

Transient natural convection in water subjected to density inversion was considered by Forbes and Cooper [13]. In their study, water, confined laterally and underneath by rigid insulating walls, was initially set at a uniform temperature and then the upper surface boundary condition was suddenly changed. Since the temperature gradient is applied vertically in the water layer, this problem is commonly classified as 'Rayleigh–Bénard instability' problem. The effect of maximum density on the transient natural convection in an enclosed rectangular cavity was also investigated by Vasseur and Robillard [14], and Robillard and Vasseur [15, 16]. They found that the convective heat

† Current address: Department of Mechanical Engineering, Aeronautical Engineering and Mechanics, Rensselaer Polytechnic Institute, Troy, NY, U.S.A.

‡ Corresponding author.

NOMENCLATURE

A	aspect ratio, H/L
g	gravitational acceleration
h	heat transfer coefficient
H	enclosure height
k	thermal conductivity
L	enclosure length
Nu	Nusselt number
p	pressure
P	dimensionless pressure
Pr	Prandtl number
Ra	Rayleigh number
T	temperature
T_0	temperature with maximum density
ΔT	temperature difference, $T_h - T_c$
$\mathbf{u}$	velocity vector, $\{u, v\}$
$\mathbf{U}$	dimensionless velocity vector $\{U, V\}$
U, V	dimensionless velocities in X and Y coordinates
x, y	coordinates
X, Y	dimensionless coordinates.

Greek symbols

θ	dimensionless temperature
κ	thermal diffusivity
μ	dynamic viscosity
ν	kinematic viscosity
ρ	density
ρ_0	maximum density
ψ	stream function
Ψ	dimensionless stream function.

Subscripts

c	cold
h	hot
l	liquid.

transfer, flow pattern and temperature profile can be greatly influenced by the presence of density maximum in the convective fluid. More recently, Oosthuizen and Paul [17] performed numerical research for a similar problem.

The present study aims at revealing the effect of density inversion on transient natural convection in water in a rectangular enclosure for Rayleigh numbers up to 10^6. Transient behavior of the temperature field and fluid flow is displayed graphically. The investigation is performed in a wide range of aspect ratio, from 0.25 to 10.

2. MATHEMATICAL FORMULATION

The geometry considered is a two-dimensional water layer confined by two horizontal impermeable and adiabatic rigid walls and two vertical walls maintained at different temperatures (Fig. 1). The fluid is initially at rest and isothermal at temperature T_0 ($T_0 = 3.98°C$) the maximum density temperature for water. At time $t = 0$, the right sidewall is abruptly cooled to the temperature T_c ($T_c = 0°C$) and maintained at this temperature thereafter. At the same time a temperature jump is applied to the left wall heated to T_h ($T_h \geqslant 3.98°C$). Thus, two vertical water sublayers are formed with opposite density gradients: at the left $\partial\rho/\partial x > 0$ and at the right $\partial\rho/\partial x < 0$. These two sublayers are separated by the maximum density plane. The flow is assumed to be Newtonian, two-dimensional and incompressible. The governing equations are the continuity, momentum and energy equations:

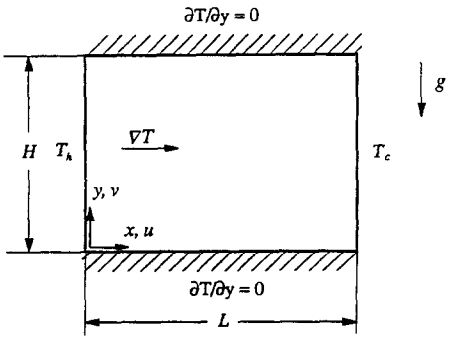

FIG. 1. Schematic configuration of the problem and coordinate system.

$$\nabla \cdot \mathbf{u} = 0 \tag{1}$$

$$\frac{\partial \mathbf{u}}{\partial t} + \mathbf{u} \cdot \nabla \mathbf{u} = -\frac{1}{\rho_0}\nabla p + \nu \nabla^2 \mathbf{u} + \frac{\rho}{\rho_0}\mathbf{g} \tag{2}$$

$$\frac{\partial T}{\partial t} + \mathbf{u} \cdot \nabla T = \kappa \nabla^2 T \tag{3}$$

where $\mathbf{u}$ is the velocity vector, ν the kinetic viscosity, T the temperature, p the pressure, t the time, ρ_0 the maximum density at T_0 ($= 3.98°C$ for water), $\mathbf{g} = g\mathbf{e}$ the gravity acceleration pointing in negative y direction.

There are several models for predicting the density–temperature behavior of water around the maximum density region. A parabolic density–temperature relationship is given by Debler [18]:

$$\frac{\rho}{\rho_0} = 1.0 - \gamma(T - T_0)^2 \tag{4}$$

where $\gamma = 8.000216 \times 10^{-6}\ (°C)^{-2}$. Later, by adding a cubic term in equation (4), this model was expanded to increase the temperature range from 0 to 30°C [19],

$$\frac{\rho}{\rho_0} = 1.0 - \gamma_1 (T - T_0)^2 + \gamma_2 (T - T_0)^3. \quad (5)$$

Gebhart and Mollendorf [20] proposed the following density equation:

$$\frac{\rho(T, s, p)}{\rho_0(s, p)} = 1.0 - \alpha(s, p) |T - T_0(s, p)|^{q(s,p)}. \quad (6)$$

The density variation is fitted in temperature, salinity, and pressure ranges to 20°C, 40‰ and 1000 bars absolute, respectively. For pure water under 1 atmosphere, $\alpha(0, 1) = 9.297173 \times 10^{-6}$ (°C), $T_m(0, 1) = 4.029325$°C and $q(0, 1) = 1.894816$. It is to be noted that the value of $T_m(0,1)$ obtained by regression is not exactly either of the often quoted values, 3.98°C or 4°C. Though equation (4) is claimed to be most accurate for the temperature range 0–8°C [18], the difference of the calculated values from equations (4) and (6) for the present interested temperature range (0–12°C) is found to be negligible small (<0.005%). Hence, equation (4) is used in this study for its simplicity.

The no-slip boundary condition is imposed at all rigid walls. The initial and boundary conditions are specified as follows:

(i) for time $t < 0$,

$$\mathbf{u} = 0; \quad T = T_0 \ \forall x, \quad \forall y \quad (7)$$

(ii) for $t \geqslant 0$,

$$\begin{aligned} &\mathbf{u} = 0; \quad T = T_h \quad \text{at } x = 0 \\ &\mathbf{u} = 0; \quad T = T_c \quad \text{at } x = L \\ &\mathbf{u} = 0; \quad \frac{\partial T}{\partial y} = 0 \quad \text{at } y = 0; y = H. \end{aligned} \quad (8)$$

The dimensionless variables (geometry, velocity, temperature, pressure and time) are introduced as follows:

$$\begin{aligned} &X = \frac{x}{L}; \qquad Y = \frac{y}{L} \\ &\mathbf{U} = \frac{\mathbf{u}}{\frac{\kappa}{L}\sqrt{(Ra\,Pr)}}; \qquad \theta = \frac{T - T_0}{T_h - T_c} \\ &P = \frac{p}{\frac{\mu\kappa}{L^2}\sqrt{(Ra\,Pr)}}; \qquad \tau = \frac{t}{\frac{L^2}{\kappa}\sqrt{(Ra\,Pr)}} \end{aligned} \quad (9)$$

where L is the enclosure length, κ the thermal diffusivity, and μ the dynamic viscosity. The Rayleigh number, Ra, and the Prandtl number, Pr, are defined by

$$Ra = \frac{g\gamma(T_h - T_c)^2 L^3}{\kappa\nu} \quad (10)$$

$$Pr = \frac{\nu}{\kappa}. \quad (11)$$

Thus, with the definitions in (9), the dimensionless governing equations expressing conservation of mass, momentum, and energy are written as:

$$\nabla \cdot \mathbf{U} = 0 \quad (12)$$

$$\sqrt{\frac{Ra}{Pr}}\left(\frac{\partial \mathbf{U}}{\partial \tau} + \mathbf{U} \cdot \nabla \mathbf{U}\right) = -\nabla P + \nabla^2 \mathbf{U} - \sqrt{\frac{Ra}{Pr}}\theta^2 \mathbf{e} \quad (13)$$

$$\sqrt{(Ra\,Pr)}\left(\frac{\partial \theta}{\partial \tau} + \mathbf{U} \cdot \nabla \theta\right) = \nabla^2 \theta. \quad (14)$$

From equation (13) it can be seen that the buoyancy effect is characterized by the ratio of two dimensionless parameters: Ra and Pr. In this study, Pr is fixed at 11.573 corresponding to the maximum density temperature $T_0 = 3.98$°C.

The heat transfer rate at the vertical walls is described by the Nusselt number, which is a function of both time and space. In terms of dimensionless parameters the local Nusselt number is defined as:

$$Nu = \left|\frac{\partial \theta}{\partial X}\right|_{X = 0, 1}. \quad (15)$$

The average Nusselt number is the integral of the local Nusselt number over the length of the vertical wall

$$\overline{Nu} = \frac{1}{A}\int_0^A \left|\frac{\partial \theta}{\partial X}\right|_{X = 0, 1} \mathrm{d}Y. \quad (16)$$

The dimensionless stream function, Ψ, is defined as:

$$U = \frac{\partial \Psi}{\partial Y}; \quad V = -\frac{\partial \Psi}{\partial X}. \quad (17)$$

Ψ is related to dimensional stream function ψ as:

$$\Psi = \frac{\psi}{\kappa(Ra\,Pr)^{1/2}}. \quad (18)$$

3. NUMERICAL SOLUTIONS

The finite element method is employed to solve the governing equations (12)–(14) along with the appropriate initial and boundary conditions. This FEM scheme uses a weak Galerkin formulation with a pressure determined by a penalty approach [21]:

$$P = \frac{1}{\lambda}(\nabla \cdot \mathbf{U}) \quad (19)$$

where the penalty parameter λ is very small and $\lambda = O(10^{-8})$ in this study. Equation (19) allows pressure to be eliminated from the momentum equations.

According to aspect ratio different nonuniform meshes, ranging from 60×21 (121×43 grid points) to 22×61 (45×121 grid points), were adopted. The finer meshes were graded toward the hot and cold walls. For a square cavity ($A = 1$), the mesh sensitivity study has shown that 43×43 grid points is adequate

Table 1. Grid point independence study for $\Delta T = 12$ C

Grid	Ra	Nu	Ra	Nu
11×11	5×10^4	2.8062	10^5	3.5566
21×21		2.6916		3.3440
35×35		2.6744		3.3092
43×43		2.6722		3.3045
55×55		2.6709		3.3016

(Table 1). A small time step is required to investigate the transition from oscillatory transient flow to steady-state. A time step $\Delta\tau$ ranges from 0.001 to 0.05, depending on the stage of the transient process.

Two nonlinear iterative solution techniques, Successive Substitution (i.e. Picard iteration) and Newton–Raphson, are combined to solve the Navier–Stokes and energy equations. Thus, the first use of the Successive Substitution method with a larger radius of convergence but possibly slower convergence rate can bring the solution vector within the radius of convergence of the Newton–Raphson method, and consequently, can result in substantial savings of computer resources. To assure transient solution convergence at each load (i.e. Rayleigh number) level, the solution vectors (temperature, velocity, etc.) of the first time step (usually $\tau = 0$) are used as initial guess for the next time step until a desired time (e.g. $\tau = 300$) is reached. This incremental approach is considered a more efficient way of implementing a Newton-based method [21].

Two variables as convergence criteria are the solution vector s_i (indicating iteration i) and the residual vector $R(s_i)$. Realistic convergence criteria are:

$$\frac{\|\Delta s_i\|}{\|s_i\|} \leqslant \varepsilon_s \tag{20}$$

$$\frac{\|R(s_i)\|}{\|R_0\|} \leqslant \varepsilon_F \tag{21}$$

where ε_s and ε_F are small quantities and set to 10^{-4} in this study, $\|-\|$ is the Euclidean norm. The combination of these two checks has proven to provide an effective overall convergence criterion for all occurring situations.

4. RESULTS AND DISCUSSION

4.1. *Evolutions of flow pattern and temperature field*

The transient convective evolutions of the temperature field and convective flow pattern for $\Delta T = 3.98$, 8 and 12°C are presented in Figs. 2–4, respectively. For the case of $\Delta T = 3.98$°C, since the maximum density plane coincides with the hot wall, the density gradient along the X-direction is negative and monotonic. Note that, unlike in regular natural convection cases where convective flows start at the hot wall, for a water layer subjected to the temperature range 0 C $= T_c < T_h \leqslant 3.98$ C convection originates from the cold side wall. At early times, while the flow develops as a weak recirculation near the cold wall the isotherms are nearly parallel indicating conduction dominated heat transfer. The convection develops in the form of a thermal plume along the upper surface. At $\tau = 50$, though the convective flow is almost fully-developed, the thickness of the thermal boundary layer at the cold wall is about the same as that at $\tau = 2.5$ (Fig. 2). In this case, only one single anti-clockwise-rotating convective roll cell is observed.

At $\Delta T = 8$°C, the density gradient is approximately symmetric with respect to the vertical mid-plane. Convection is seen to develop from the two vertical walls with almost equal strength (Fig. 3). This behavior is similar to the problem with two immiscible isodensity liquids separated by a vertical interface. At $\tau = 50$, the symmetric convective cells show a relatively slow flow and isothermal region at the lower centerpart of the enclosure.

Increasing ΔT to 12 C the maximum density plane develops close to the cold wall. The interaction between 'regular' natural convection (from the hot wall) and 'density inversion' convection (from the cold wall) results in complex flow and temperature fields as a function of time. It can be seen from Fig. 4 that the density of isotherms developing at the hot wall is higher than at the cold wall. As two temperature plumes meet at the top of the enclosure they expand to the bottom in a complicated slanted manner. The streamlines show that the convective flow generated at the cold wall is gradually compressed into the lower right-hand corner. Two convective cells are separated by the $\Psi = 0$ plane at all times. The convective flow generated at the hot wall dominates the flow field all the time.

The behavior of transient mean Nusselt number for a square enclosure along a vertical wall at $Ra = 10^6$ is displayed in Fig. 5. It shows that, after application of a step function temperature jump at the beginning of the process, for all ΔT cases, Nusselt numbers decrease steeply within a short time ($\tau < 5$). This result agrees well with that predicted by the one-dimensional transient conduction model [22–24]. At the point where the heat transfer mode changes from conduction-dominated to convection-dominated at larger times, the slopes of the Nu curves become flat, and, at very long time, approach constant values. The flow characteristic values at each time step are presented in Table 2 to reflect the magnitude of the heat transfer rate and intensity of convection under different ΔT conditions.

From Fig. 5, it is also found that the mean Nusselt number for the convective flow with bicellular cells (e.g. $\Delta T = 12$°C) is always lower than that with a unicellular cell (e.g. $\Delta T = 3.98$°C). This is because of the presence of the additional thermal resistance between two convective roll cells. When these two cells reach equal size, the thermal resistance is maximized and thus the heat transfer rate is minimized.

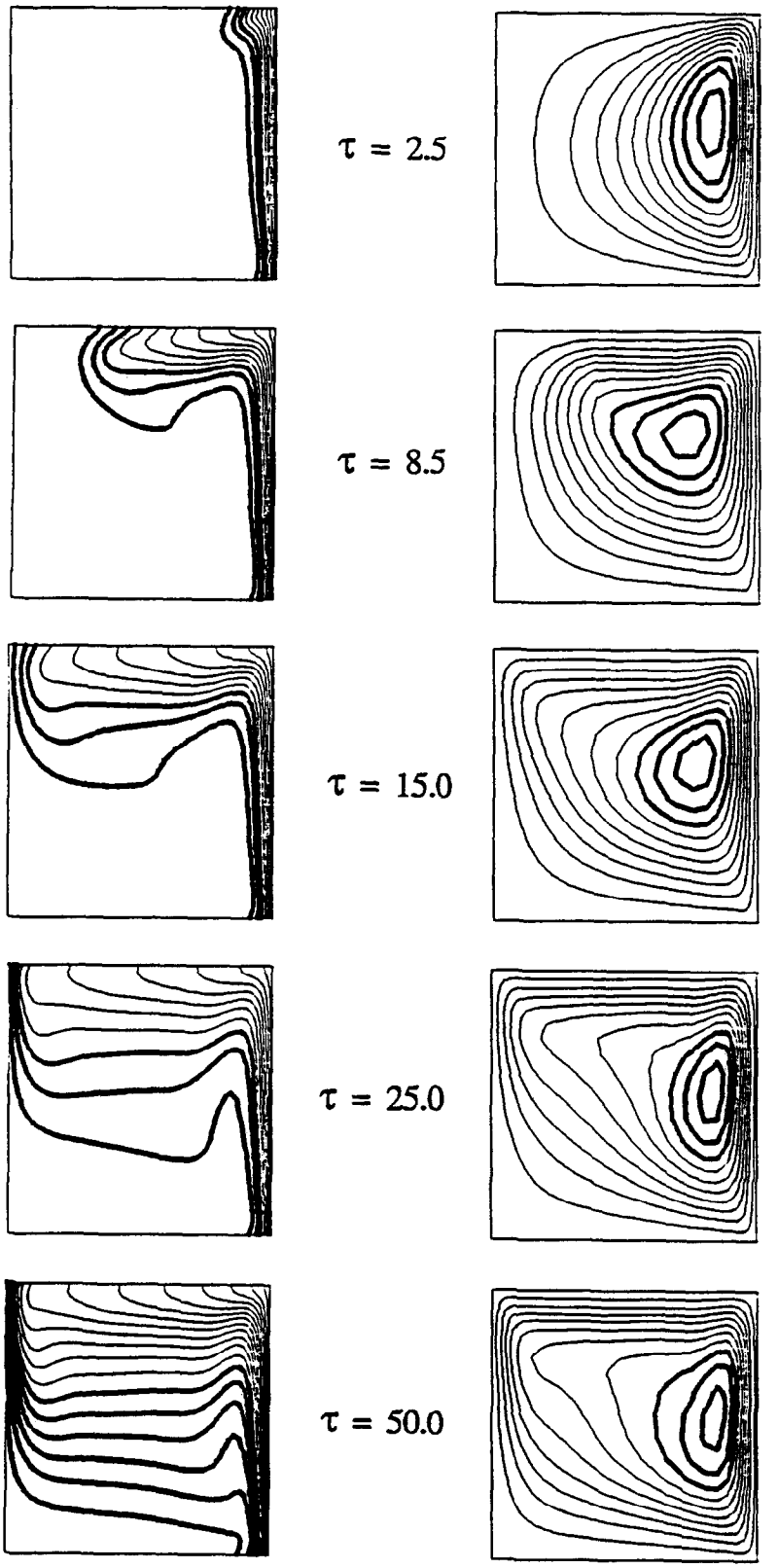

FIG. 2. Evolution of the temperature field (left column) and convective flow pattern (right column) in transient convection for $\Delta T = 3.98°C$ and $Ra = 10^6$ (monotonic density gradient).

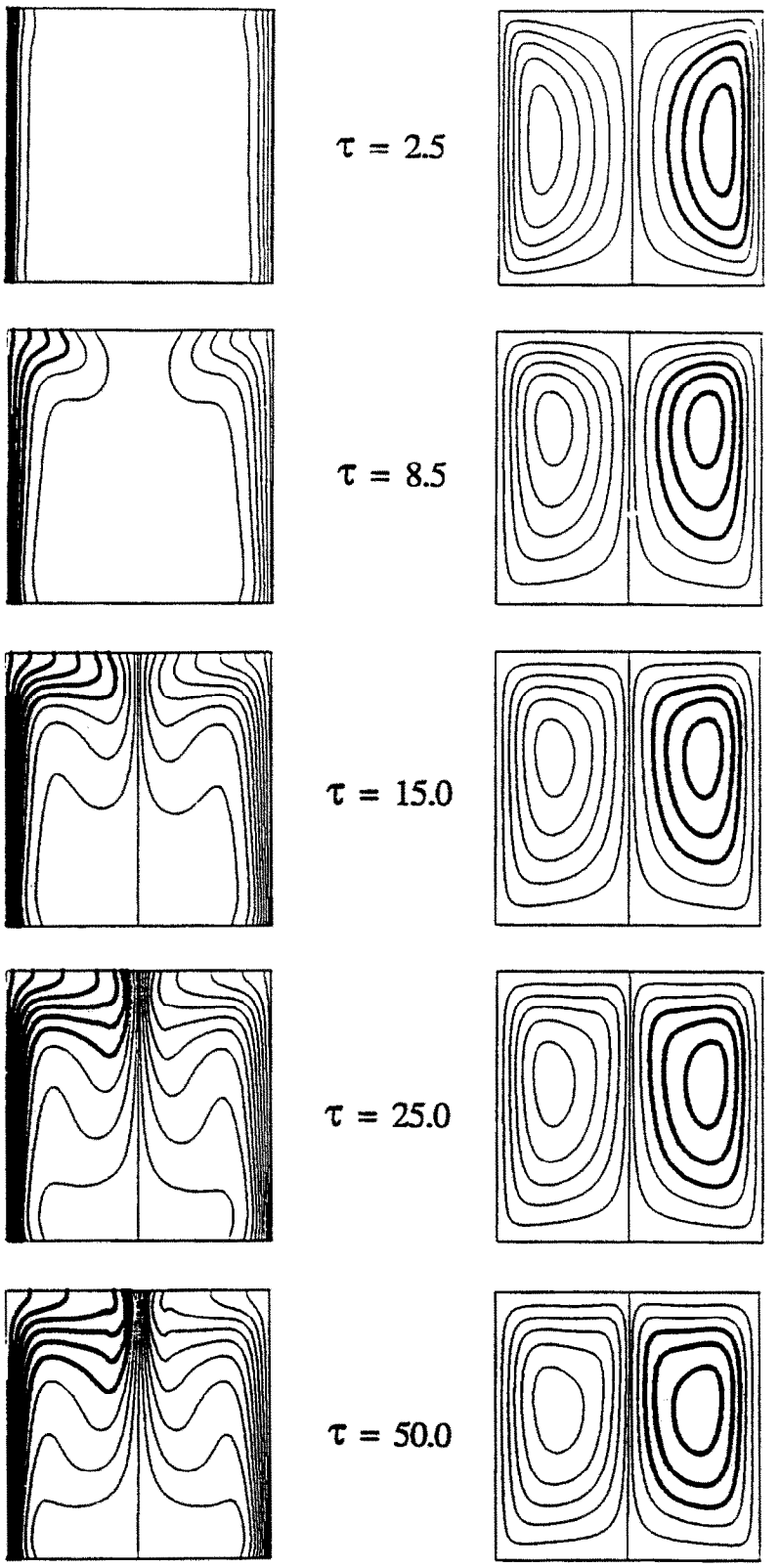

FIG. 3. Evolution of the temperature field (left column) and convective flow pattern (right column) in transient convection for $\Delta T = 8°C$ and $Ra = 10^6$.

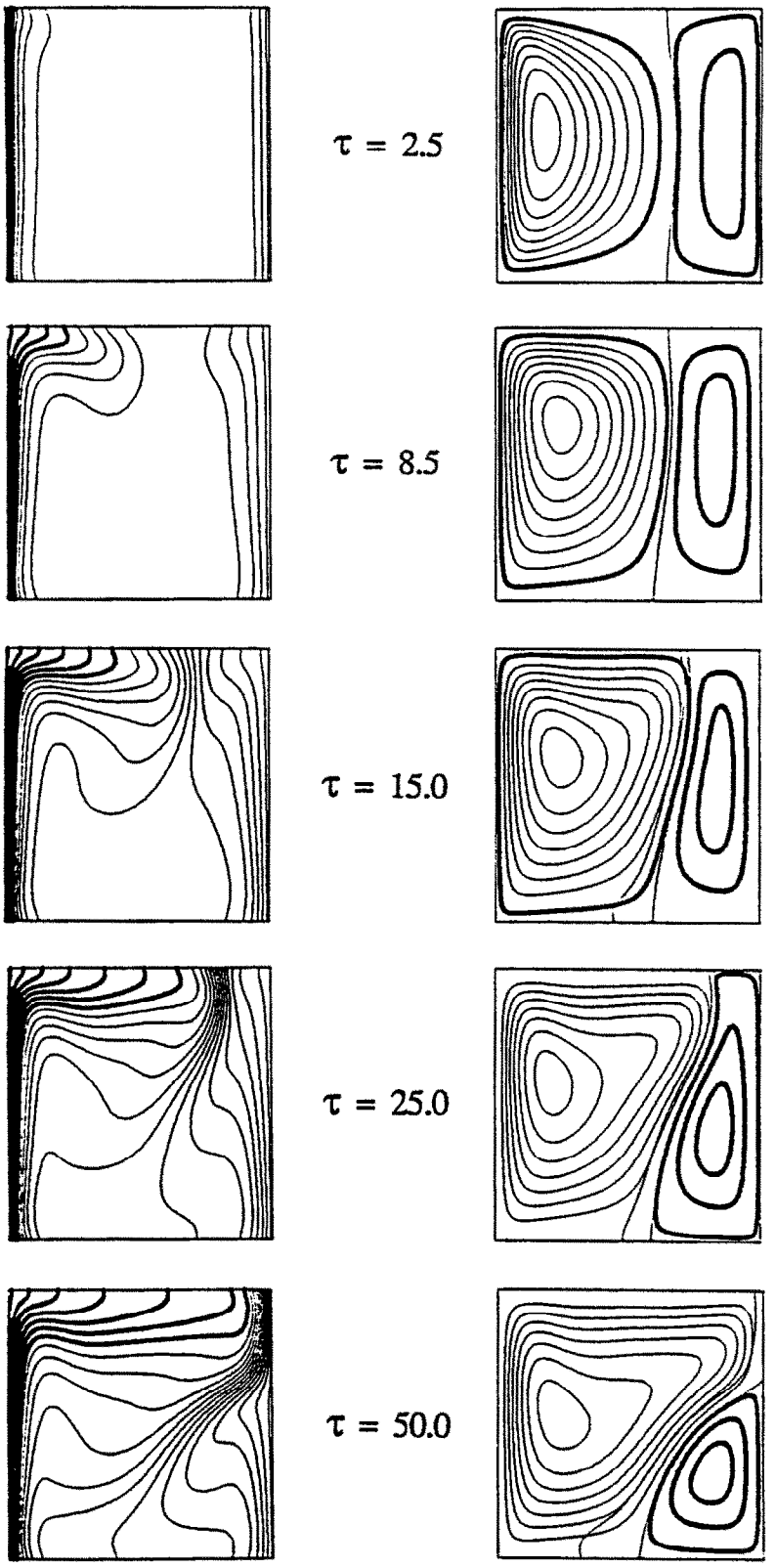

FIG. 4. Evolution of the temperature field (left column) and convective flow pattern (right column) in transient convection for $\Delta T = 12°C$ and $Ra = 10^6$.

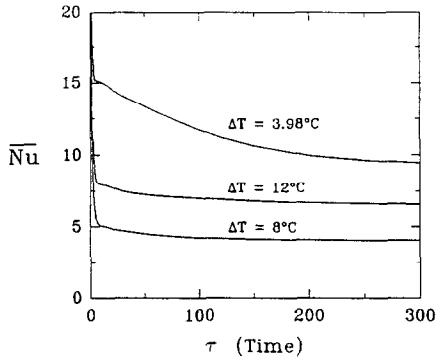

FIG. 5. Effect of temperature difference on transient mean Nusselt number at $Ra = 10^6$ and $A = 1$. $\Delta T = 3.98$°C (cold wall); $\Delta T = 8$°C (hot wall); $\Delta T = 12$°C (hot wall).

4.2. *Time-dependence of local Nusselt number and vertical velocity component for A = 1*

Transient local Nusselt numbers inform on the evolution of the thermal field in the heated wall region. Figure 6 presents the development of the local Nusselt number profile for three values of ΔT. At the early stage of the process, the transient local Nusselt numbers are nearly constant over the height of a wall, except in corner regions. As soon as convection gains strength, temperature gradients at the vertical wall decrease significantly. For large times *Nu* curves approach linear profiles. At $\tau \geqslant 300$, *Nu* curves coincide closely with steady state conditions ($\tau \to \infty$).

Table 2. Convective flow characteristics for $A = 1$ ($Ra = 10^6$)

ΔT	τ	*Nu*	Ψ_{max} ($\times 10^3$)	Ψ_{min} ($\times 10^3$)
3.98	2.5	16.645	7.339	0
	8.5	15.079	12.789	0
	15.0	14.859	10.906	0
	25.0	14.266	8.225	0
	50.0	13.347	7.369	0
	100.0	11.739	6.668	0
	150.0	10.614	6.462	0
	200.0	9.972	6.328	0
	300.0	9.461	6.158	0
	∞	9.270	6.071	0
8.0	2.5	7.902	1.735	−1.775
	8.5	5.131	5.729	−5.826
	15.0	4.991	5.433	−5.516
	25.0	4.772	4.823	−4.890
	50.0	4.505	5.015	−5.119
	100.0	4.215	5.473	−5.530
	150.0	4.119	5.604	−5.649
	200.0	4.087	5.632	−5.703
	300.0	4.067	5.635	−5.727
	∞	4.059	5.303	−5.288
12.0	2.5	10.676	0.632	−3.262
	8.5	8.002	2.252	−8.602
	15.0	7.880	2.295	−7.837
	25.0	7.603	2.255	−6.767
	50.0	7.261	2.392	−6.717
	100.0	6.985	2.261	−6.031
	150.0	6.806	2.105	−5.683
	200.0	6.691	1.925	−5.529
	300.0	6.574	1.733	−5.418
	∞	6.516	1.816	−5.228

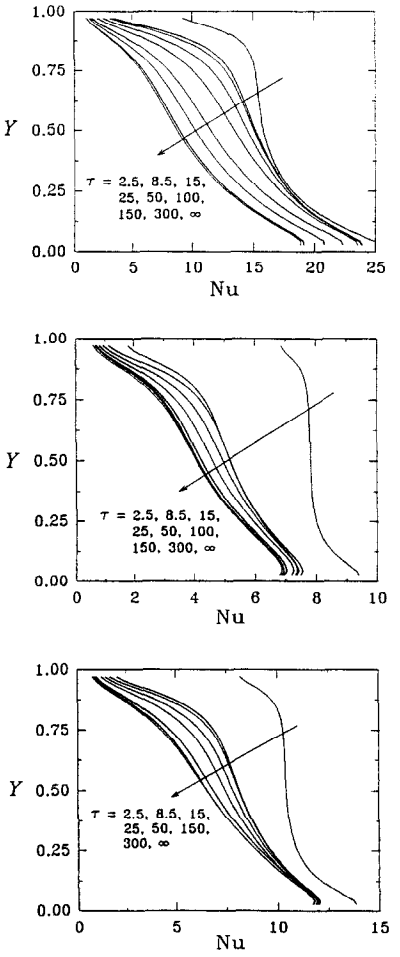

FIG. 6. Time-dependent local Nusselt number distribution at $Ra = 10^6$ and $A = 1$. Top: $\Delta T = 3.98$°C (cold wall); middle: $\Delta T = 8$°C (hot wall); bottom: $\Delta T = 12$°C (hot wall).

The development of transient vertical velocity profiles at $Y = 0.5$ is depicted in Fig. 7. The plots demonstrate that ΔT and T_c, which determine the position of the maximum density plane, essentially alter the *V*-velocity distribution along the *X*-axis. For a single convective roll cell ($\Delta T = 3.98$°C) the velocity profile is initially established near the cold wall and develops toward the hot wall as $\tau > 15$. In the case of $\Delta T = 8$°C, once natural convection starts, the *V*-velocity reaches its peaks near the vertical walls and maintains this character thereafter. As time increases the flow develops in the core region. Similar behavior is seen for $\Delta T = 12$°C but with asymmetric shift toward the hot wall. The evolution of the flow in the core region and in the cold wall region exposes more complicated features due to the strong influence of the second convective roll cell confined to the lower right corner (see Fig. 4). Even at $\tau = 150$ the flow is still far from its steady state. In contrast, the heat transfer, referred to in Fig. 6, approaches its final steady state profile faster than does the flow field.

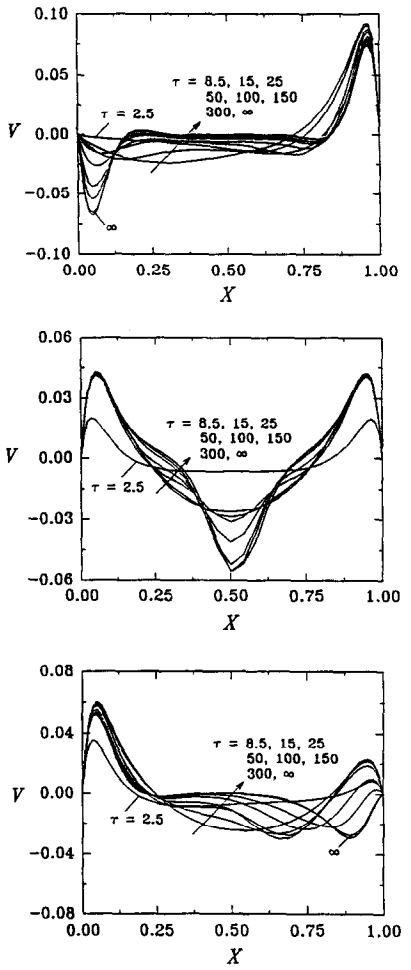

FIG. 7. Time dependent vertical velocity profile at $Y = 0.5$. Top: $\Delta T = 3.98°C$; middle: $\Delta T = 8°C$; bottom: $\Delta T = 12°C$.

of the enclosure but is briskly compressed into the lower right corner. As time increases this cell expands again and finally finds its equilibrium size in the lower right corner.

Figure 10 shows the effect of aspect ratio on transient mean Nusselt number for $\Delta T = 12°C$ and $Ra = 10^6$. In all cases Nu values decrease vs time and approach steady-state values. No oscillations are observed in heat transfer. It is worth noting that, at $A = 1$, for $\tau > 90$, the heat transfer rate is highest compared to other A-values. For $A > 1$ this is a consequence of the increased shear stress at vertical walls which impede changes in temperature and flow fields at the side walls. For the cases of $A < 1$ the reduced heat transfer is directly related to smaller H, i.e. a reduced effective buoyancy force. In the asymptotic case of $A \ll 1$, only the heat transfer mode is conduction. The values of $\overline{Nu}$, Ψ_{max} and Ψ_{min} for $A < 1$ and $A > 1$ are given in Tables 3(a) and 3(b), respectively.

It is interesting to note from Fig. 10 that during the transition from a conduction to a convection dominated mode the Nusselt numbers at $A > 1$ pass through local minima. Corresponding to this minimum in Nusselt number, the thickness of the boundary layer reaches its maximum value. This phenomenon agrees well with results by Patterson and Imberger [2], and Nicolette *et al.* [6]. However, for $A < 1$ $\overline{Nu}$ decreases smoothly with time. This character can be explained: in the aspect ratio study, since both Ra and ΔT are fixed, the enclosure length, L, is also specified. Thus, the change of aspect ratio is based on the variation of the thickness of the whole water layer, H. For a case with small aspect ratio (small H) convection requires more time to develop than in a narrow vertical cavity.

4.3. *Aspect ratio effect on natural convection*

In internal flow, the aspect ratio is an important parameter because it changes the flow structure. To study the effect of aspect ratio on transient natural convection computations were carried out for $\Delta T = 12°C$ and $Ra = 10^6$ with aspect ratio varying between 0.25 and 10.

The evolutions of temperature field and convective flow pattern are displayed in Figs. 8 and 9 for $A = 0.5$ and 2, respectively. For $A = 0.5$, it is found that two convective roll cells develop independently at two vertical walls (Fig. 8). At $\tau > 25$ the thermal fields from each vertical wall compete with each other. The left flow with a higher dynamic momentum pushes the right flow toward the cold wall, as a result, the right cell is compressed. During the time interval of $50 \leqslant \tau \leqslant 150$, this compression rate reached its highest level and the right cell settles in the lower right corner.

Similar behavior can be observed for $A = 2$ (Fig. 9). During this transient process, the right roll cell displays stronger oscillation that for $A = 0.5$. The right roll cell extends initially along the whole height

Table 3.(a) Convective flow characteristics for $A < 1$ ($Ra = 10^6$ and $\Delta T = 12°C$)

A	τ	$\overline{Nu}$	Ψ_{max} ($\times 10^3$)	Ψ_{min} ($\times 10^3$)	Grid
0.25	2.5	10.591	0.225	−0.867	121 × 43
	8.5	7.905	0.456	−1.300	
	15.0	7.240	0.520	−1.289	
	25.0	6.629	0.550	−1.273	
	50.0	5.531	0.570	−1.256	
	100.0	4.318	0.609	−1.233	
	150.0	3.753	0.633	−1.214	
	200.0	3.432	0.610	−1.198	
	300.0	3.053	0.500	−1.172	
0.50	2.5	10.700	0.515	−2.018	85 × 45
	8.5	8.480	1.463	−3.627	
	15.0	8.291	1.665	−3.462	
	25.0	8.067	1.578	−3.265	
	50.0	7.561	1.294	−3.081	
	100.0	6.921	0.611	−3.040	
	150.0	6.587	0.405	−2.991	
	200.0	6.401	0.330	−2.987	
	300.0	6.257	0.292	−2.992	

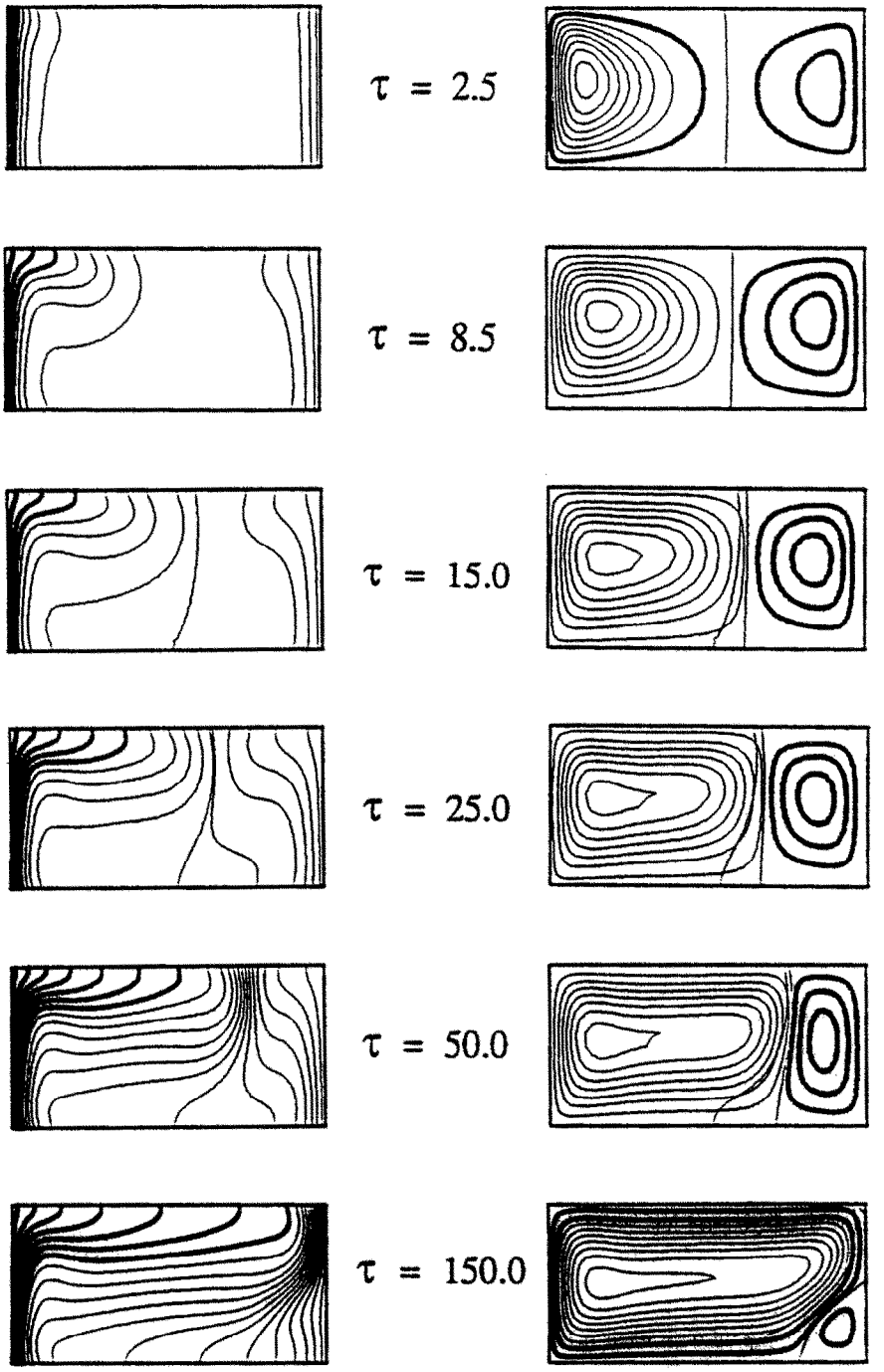

FIG. 8. Evolution of the temperature field (left column) and convective flow pattern (right column) for $A = 0.5$ at $Ra = 10^6$ and $\Delta T = 12°C$.

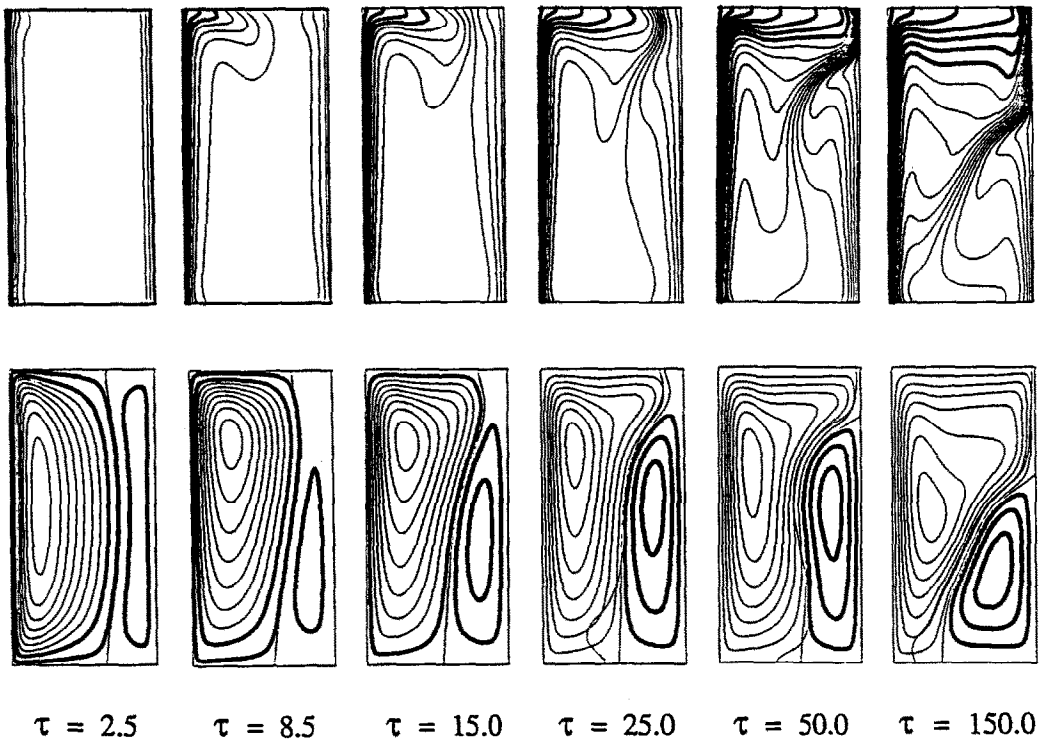

FIG. 9. Evolution of the temperature field (top) and convective flow pattern (bottom) for $A = 2$ at $Ra = 10^6$ and $\Delta T = 12°C$.

Table 3.(b) Convective flow characteristics for $A > 1$ ($Ra = 10^6$ and $\Delta T = 12°C$)

A	τ	$\overline{Nu}$	Ψ_{max} ($\times 10^3$)	Ψ_{min} ($\times 10^3$)	Grid
2	2.5	10.511	0.575	−3.829	45 × 85
	8.5	7.025	2.507	−15.930	
	15.0	7.002	4.034	−15.531	
	25.0	6.906	5.323	−12.652	
	50.0	6.699	4.565	−11.312	
	100.0	6.330	4.541	−11.339	
	150.0	6.150	4.764	−10.724	
	200.0	6.028	4.940	−10.060	
	300.0	5.913	5.152	−9.401	
4	2.5	10.560	0.571	−3.947	33 × 121
	8.5	6.278	2.504	−19.262	
	15.0	6.001	3.921	−26.521	
	25.0	5.867	5.683	−21.071	
	50.0	5.603	6.820	−18.095	
	100.0	5.217	6.912	−17.847	
	150.0	5.050	7.965	−18.228	
	200.0	4.985	7.639	−17.893	
	300.0	4.956	9.169	−16.117	
10	2.5	10.403	0.572	−3.927	45 × 121
	8.5	5.750	2.498	−19.317	
	15.0	4.865	4.806	−34.643	
	25.0	4.699	7.828	−37.765	
	50.0	4.539	10.399	−33.202	
	100.0	4.364	10.363	−33.558	
	150.0	4.242	11.940	−34.339	
	200.0	4.129	12.750	−34.056	
	300.0	4.005	13.538	−33.999	

5. CONCLUSIONS

The effect of density inversion on transient natural convection in a water layer within a rectangular enclosure is studied numerically by FEM methods. The results elucidate that the position of the maximum density plane has a determining effect on the transient convective process. For $\Delta T = 3.98°C$, the flow is observed to develop at the cold wall to form unicellular flow. As $\Delta T > 3.98°C$, with $T_c = 0°C$, the interaction between regular natural convection, originated at the hot wall, and convection due to density

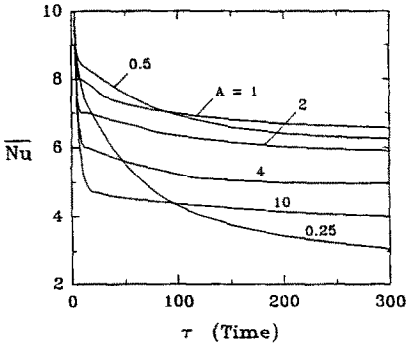

FIG. 10. Aspect ratio effect on transient mean Nusselt number for $\Delta T = 12°C$ and $Ra = 10^6$.

inversion, originated at the cold wall, makes the flow field more complicated. For a square enclosure ($A = 1$), the heat transfer rate is found to be bound by two extreme cases: the maximum value obtained at $\Delta T = 3.98°C$ with a single convection cell, and the minimum value at $\Delta T = 8°C$, with two convective cells which are symmetric to the central vertical density inversion plane.

The temporal behavior of heat transfer and vertical velocity profile suggest that during early stages of the transient process ($\tau < 5$), conduction is dominant, then the heat transfer mode changes from conduction to convection-dominated, similar to monotonic density fluids. In all cases the convective flow reaches steady state at dimensionless approximate time of $\tau \sim 300$.

The aspect ratio has shown its significant effect on the evolution of the isotherm and streamline contours. The time-dependent development of the mean Nusselt number reaches steady state at large times. During the convection-dominated process, two characteristics can be identified: (a) for $A > 1$, transient mean Nusselt numbers pass through a local minimum during the transition from a conduction-dominated to a convection-dominated heat transfer mode. A strong spatial oscillation of the roll cells occurs before reaching steady state. (b) For $A < 1$ the heat transfer rate diminishes smoothly with time.

Acknowledgements—The authors would like to acknowledge the support of this work from NASA under Grant NAG3-1094.

REFERENCES

1. F. Landis and H. Yanowitz, Transient natural convection in a narrow vertical cell, *Proc. 3rd Int. Heat Transfer Conf.*, Vol. 2, pp. 139–151 (1966).
2. J. Patterson and J. Imberger, Unsteady natural convection in a rectangular cavity, *J. Fluid Mech.* **100,** 65–86 (1980).
3. A. Bejan, A. Al-Homoud and J. Imberger, Experimental study of high-Rayleigh-number convection in a horizontal cavity with different end temperature, *J. Fluid Mech.* **109,** 283–299 (1981).
4. S. M. Han, A transient numerical analysis of high Rayleigh number convection in a different heated square cavity, ASME Paper 84-HT-57 (1984).
5. G. N. Ivey, Experiments on transient natural convection in a cavity, *J. Fluid Mech.* **144,** 433–447 (1984).
6. V. F. Nicolette, K. T. Yang and J. R. Lloyd, Transient cooling by natural convection in a two-dimensional square enclosure, *Int. J. Heat Mass Transfer* **28,** 1721–1732 (1985).
7. J. D. Hall, A. Bejan and J. B. Chaddock, Transient natural convection in a rectangular enclosure with one heated side wall, *Int. J. Heat Fluid Flow* **9,** 396–404 (1988).
8. A. Watson, The effect of the inversion temperature on the convection of water in an enclosed rectangular cavity, *Quart. J. Mech. Appl. Math.* **25,** 423–446 (1972).
9. D. S. Lin and M. W. Nansteel, Natural convective heat transfer in a square enclosure containing water near its density maximum, *Int. J. Heat Mass Transfer* **30,** 2319–2329 (1987).
10. N. Seki, S. Fukusako and H. Inaba, Free convective heat transfer with density inversion in a confined rectangular vessel, *Wärme- und Stoffübertragung* **11,** 145–156 (1978).
11. V. S. Desai and R. E. Forbes, Free convection in water in the vicinity of maximum density, *Envir. Geophys. Heat Transfer* **4,** 41–47 (1971).
12. W. Tong and J. N. Koster, Coupling of natural convection flow across a vertical density inversion interface, *Wärme- und Stoffübertragung*, **28,** 471–479 (1993).
13. R. E. Forbes and J. W. Cooper, Natural convection in a horizontal layer of water cooled from above to near freezing, *ASME J. Heat Transfer* **97,** 47–53 (1975).
14. P. Vasseur and L. Robillard, Transient natural convection heat transfer in a mass of water cooled through 4°C, *Int. J. Heat Mass Transfer* **23,** 1195–1205 (1980).
15. L. Robillard and P. Vasseur, Transient natural convection heat transfer of water with maximum density and supercooling, *ASME J. Heat Transfer* **103,** 528–534 (1981).
16. L. Robillard and P. Vasseur, Convective response of a mass of water near 4°C to a constant cooling rate applied on its boundaries, *J. Fluid Mech.* **118,** 123–141 (1982).
17. P. H. Oosthuizen and J. T. Paul, Unsteady free convective flow in an enclosure containing water near its density maximum, HTD-Vol. 140, pp. 83–91 (1990).
18. W. R. Debler, On the analogy between thermal and rotational hydrodynamic stability, *J. Fluid Mechanics* **24,** 165–176 (1966).
19. Z.-S. Sun, C. Tien and Y.-C. Yen, Thermal instability of a horizontal layer of liquid with maximum density, *A.I.Ch.E.Jl* **15,** 910–915 (1969).
20. B. Gebhart and J. C. Mollendorf, A new density relation for pure and saline water, *Deep-Sea Res.* **24,** 831–848 (1977).
21. FIDAP, Fluid Dynamics International, Inc., Evanston, IL (1992).
22. B. Gebhart, Transient natural convection from vertical elements, *ASME J. Heat Transfer* **83,** 61–70 (1961).
23. B. Gebhart, Transient natural convection from vertical elements—appreciable thermal capacity, *ASME J. Heat Transfer* **85C,** 10–14 (1963).
24. R. J. Goldstein and D. G. Briggs, Transient free convection about vertical plates and cylinders, *ASME J. Heat Transfer* **86C,** 490–500 (1964).